Spatiotemporal dynamics of neocortical excitation and inhibition during human sleep

Adrien Peyrache[a,b], Nima Dehghani[a], Emad N. Eskandar[c,d], Joseph R. Madsen[e,f], William S. Anderson[f], Jacob A. Donoghue[g], Leigh R. Hochberg[g,h,i,j], Eric Halgren[k], Sydney S. Cash[g,1], and Alain Destexhe[a,1]

[a]Unité de Neurosciences, Information, et Complexité, Centre National de la Recherche Scientifique, 91198 Gif-sur-Yvette, France; [b]Center for Molecular and Behavioral Neuroscience, Rutgers, The State University of New Jersey, Newark, NJ 07102; [c]Department of Neurosurgery, Massachusetts General Hospital and Harvard Medical School, Boston, MA 02114; [d]Nayef Al-Rodhan Laboratories for Cellular Neurosurgery and Neurosurgical Technology, Massachusetts General Hospital and Harvard Medical School, Boston, MA 02114; [e]Department of Neurosurgery, Children's Hospital and Harvard Medical School, Boston, MA 02115; [f]Department of Neurosurgery, Brigham and Women's Hospital and Harvard Medical School, Boston, MA 02115; [g]Department of Neurology, Massachusetts General Hospital and Harvard Medical School, Boston, MA 02114; [h]Institute for Brain Science, Brown University, Providence, RI 02912; [i]Rehabilitation Research and Development Service, Department of Veterans Affairs, Providence, RI 02908; [j]School of Engineering, Brown University, Providence, RI 02912; and [k]Departments of Radiology, Neurosciences, and Psychiatry, University of California at San Diego, La Jolla, CA 92037

Edited by N. Kopell, Boston University, Boston, MA, and approved December 21, 2011 (received for review June 20, 2011)

Intracranial recording is an important diagnostic method routinely used in a number of neurological monitoring scenarios. In recent years, advancements in such recordings have been extended to include unit activity of an ensemble of neurons. However, a detailed functional characterization of excitatory and inhibitory cells has not been attempted in human neocortex, particularly during the sleep state. Here, we report that such feature discrimination is possible from high-density recordings in the neocortex by using 2D multielectrode arrays. Successful separation of regular-spiking neurons (or bursting cells) from fast-spiking cells resulted in well-defined clusters that each showed unique intrinsic firing properties. The high density of the array, which allowed recording from a large number of cells (up to 90), helped us to identify apparent monosynaptic connections, confirming the excitatory and inhibitory nature of regular-spiking and fast-spiking cells, thus categorized as putative pyramidal cells and interneurons, respectively. Finally, we investigated the dynamics of correlations within each class. A marked exponential decay with distance was observed in the case of excitatory but not for inhibitory cells. Although the amplitude of that decline depended on the timescale at which the correlations were computed, the spatial constant did not. Furthermore, this spatial constant is compatible with the typical size of human columnar organization. These findings provide a detailed characterization of neuronal activity, functional connectivity at the microcircuit level, and the interplay of excitation and inhibition in the human neocortex.

spontaneous activity | ensemble recordings | single unit | functional dynamics

From columnar microcircuits (1–3) to higher-order neuronal functional units, neocortical dynamics are characterized by a large range of spatial and temporal scales (4, 5). Recent technical improvements have allowed the nature of these dynamics in the human brain to be directly explored: Single-neuron activity in conjunction with local field potentials (LFPs) can be detected from the cerebral cortex and hippocampus in the course of intense monitoring of brain activity before surgical treatment of epileptic foci (6). Modern electrode systems provide the possibility of extracellular recordings of neuronal ensembles by using either microwires (7) or high-density microelectrode arrays (8, 9). Prior efforts have demonstrated excellent recordings of single-neuron activity in human cerebral cortex (10–12).

Separation of units between "regular-spiking" (RS) and "fast-spiking" (FS) neurons, presumably excitatory (pyramidal) and inhibitory (interneuron) cells, respectively, is commonly practiced in animal experiments. In the neocortex of various mammalian species, RS and FS cells can be reliably separated based on spike waveform, duration, and firing rates (13, 14). Similar criteria were also used to successfully separate units into putative pyramidal (Pyr) cells and inhibitory interneurons (Int) in human hippocampus (15). Two recent studies have used morphological features to distinguish between these two classes of neurons (16, 17). However, the network interaction between these types of morphofunctional discriminated units has still largely not been investigated. Neuronal correlations have been shown to decay with space in primary visual cortex, possibly caused by the highly structured nature of inputs (18). In parallel, it has been shown that, in the rodent hippocampus, at the top of cortical processing, such an effect of distance on neuronal correlations was also present and was different for excitatory and inhibitory cells (19).

The 2D high-density recordings of human neuronal activity offer a unique opportunity to study the spatiotemporal dynamics of excitation and inhibition in the neocortical network (16, 17, 20). In the present paper, we successfully categorize the extracellularly recorded units into RS and FS during sleep and show their putative excitatory or inhibitory nature based on monosynaptic connections. We also provide evidence for distinctive network dynamics for each category of these neurons during drowsiness and sleep spontaneous activity.

Results

Separation of RS and FS Cells. A sample recording of intracranial EEG, LFP, and unit recordings from the microelectrode array is shown in Fig. 1. The firing of excitatory and inhibitory cells was strongly correlated (Fig. 1*C*). By using standard methods (13, 14), those two cell types were discriminated on the basis of their action potential waveforms (*SI Materials and Methods*). The waveform half widths and valley-to-peak distributions exhibited two automatically detected well-defined clusters (Fig. 2 *A* and *B*). Other waveform features can be used and yielded the same separation (Fig. S1 *B* and *C*). Each cluster showed a distinct spike waveform (Fig. 2*C*): A short, fast-decaying action potential represents putative FS and GABAergic cells; a large and slower one depicts putative RS and glutamatergic neurons. A total of 190 RS and 46 FS cells were discriminated from three patients (four recording sessions). This ratio amounts to an 80% excitatory and 20% inhibitory distribution of cells.

This morphological clustering was validated by distinctive cell-intrinsic properties. The average firing rates showed remarkable separation between the two groups, with FS firing at higher rates

Author contributions: A.P., N.D., S.S.C., and A.D. designed research; A.P., N.D., E.N.E., J.R.M., W.S.A., J.A.D., L.R.H., E.H., S.S.C., and A.D. performed research; A.P., N.D., and A.D. analyzed data; and A.P., N.D., E.H., S.S.C., and A.D. wrote the paper.

The authors declare no conflict of interest.

This article is a PNAS Direct Submission.

[1]To whom correspondence may be addressed. E-mail: destexhe@unic.cnrs-gif.fr or scash@partners.org.

This article contains supporting information online at www.pnas.org/lookup/suppl/doi:10.1073/pnas.1109895109/-/DCSupplemental.

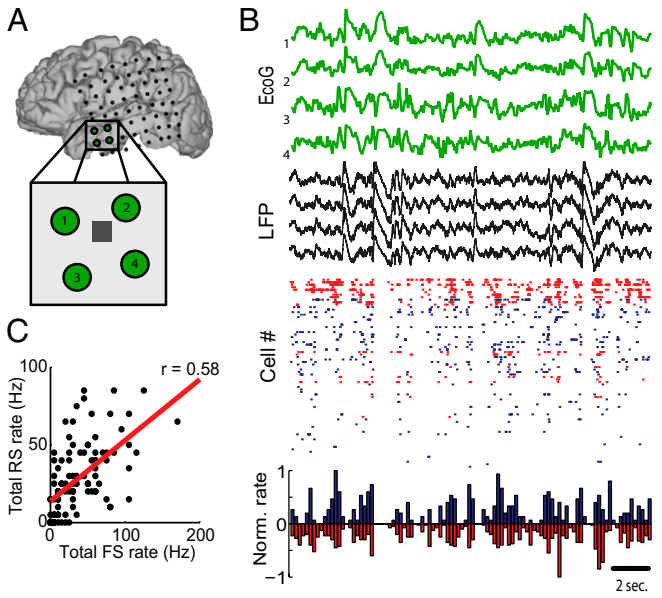

Fig. 1. (*A*) Localization of subdural electrodes (*SI Materials and Methods*) and the NeuroPort electrode array (gray square in *Inset*). (*B*) Green traces show electrocorticogram (EcoG) of the four closest contacts to the microelectrode. LFP recorded from the NeuroPort is plotted in black. Raster plot shows the pooled firing of inhibitory (red) vs. excitatory (blue) cells for this period of slow-wave sleep. Histogram shows normalized neuronal firing rate for the two groups of cells in 200-ms time bins. (*C*) Total spikes by RS and FS cells in successive 200-ms bins, plotted against each-other (same epoch as in *B*).

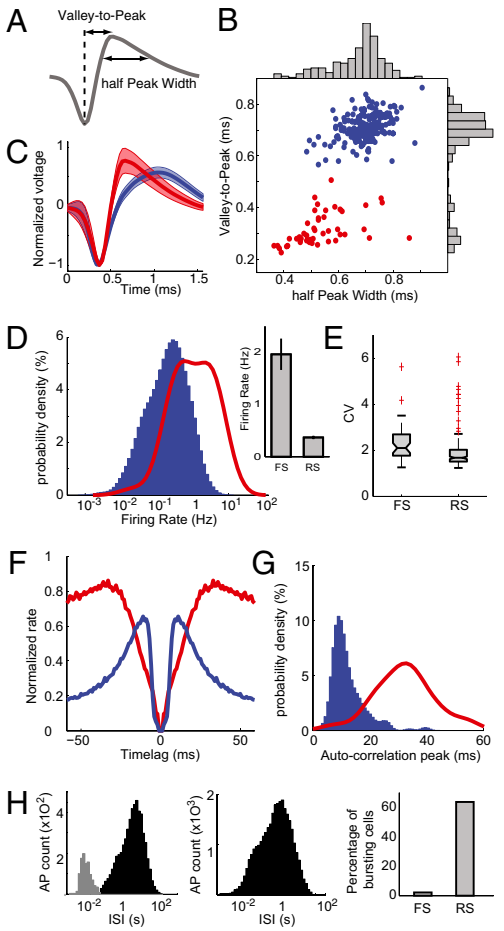

Fig. 2. Separation of FS and RS cells based on spike waveform. (*A*) Valley-to-peak and half-peak widths were the two parameters chosen to describe spike waveforms. (*B*) Each cell's average waveform is represented in the 2D space of the previous two parameters. The two clusters were identified with a *k*-means algorithm representing in red FS and in blue RS cells. (*C*) Average spike waveform for the two groups. Shading represents SD. (*D*) Probability density of firing rates for the two groups. (*Inset*) Average ± SEM. (*E*) Box plot indicating interquartile distribution of coefficients of variation (CV) of ISIs. (*F*) Average autocorrelogram normalized to maximum for each group. (*G*) Distribution of autocorrelogram modes (time of maximum peak) for each group. (*H*) Distribution of ISIs for an example RS cell (*Left*) and an FS cell (*Center*). The gray part of the distribution indicates the ISI categorized as bursts. (*Right*) Percentage of cells classified as bursty for each cell type. AP, action potentials. In *D* and *G*, the density probabilities were computed from kernel-smoothing density estimates of the actual data and displayed such that the sum over the whole displayed interval is equal to 100 for each group.

(Fig. 2*D*, $P < 10^{-10}$, one-way ANOVA). Both firing-rate distributions had a Gaussian-like shape in logarithmic x coordinates (Fig. 2*D*); therefore, firing rates can be estimated as being drawn from log-normal distribution for both cell types. FS firing rate was on average five times higher than RS cell firing rate was, which, interestingly, is comparable to the ratio of discriminated FS and RS cells in the whole dataset.

Coefficients of variation [the ratio of the SD to the mean of the interspike interval (ISI) distribution] were also significantly different for the two cell groups (Fig. 2*E*, $P < 0.01$, one-way ANOVA). Furthermore, cells could be also segregated based on their autocorrelogram (Fig. 2*F*): Int are known to have long refractory periods and show a slow rising autocorrelation. On the other hand, RS cells show sharp autocorrelograms, reflecting their shorter refractory period and their tendency to fire in bursts. The distributions of the modes (i.e., time of maximal values in the autocorrelogram) were highly distinct (Fig. 2*G*).

Finally, isolated neurons were tested for their burstiness. The histograms of the ISIs were sometimes characterized by a clear bimodality, especially when the logarithm of the ISI was considered (Fig. 2*H*, *Left* and *Center*). Cells were classified as bursty when they passed the significance level of a bootstrap-based test for bimodality (21). As displayed in Fig. 2*H*, of the population that did not have FS morphological characteristics, 64% expressed bursting behavior. Only 2% of FS (that is only one cell in the whole dataset) showed such properties.

Putative Monosynaptic Connections. Analysis of cross-correlograms between pairs of units allows the characterization of putative monosynaptic connections (13): Positive, short-latency peaks (<4 ms) are the sign of a biased tendency of the reference cell A firing just before the other cell (B) at above chance level, which would thus be the functional signature of an excitatory monosynaptic connection from cell A to cell B. Conversely, a gap in the cross-correlograms indicates an inhibitory monosynaptic connection. The expected cross-correlogram for two unrelated cells was obtained by jittering each pair of spike trains and by computing the 99% confidence interval (*SI Materials and Methods*). Cell pairs showing an excess of biased spikes occurring above this threshold were categorized as monosynaptically connected. Fig. 3*A* shows an example of a reciprocally connected putative Pyr/Int pair. Occasionally, some Pyr cells excited another target cells without any significant reciprocal connection (Fig. 3*B*).

The excitatory or inhibitory nature of the postsynaptic effect from the efferent cells was remarkably matched to their spike waveform characteristics (Fig. 3*C*). This association of synaptic effects with action potential waveforms significantly differed from chance ($\chi^2 = 33.6$, df = 2, $P < 0.0001$) and provides converging evidence for the validity of the morphofunctional dichotomy within the network.

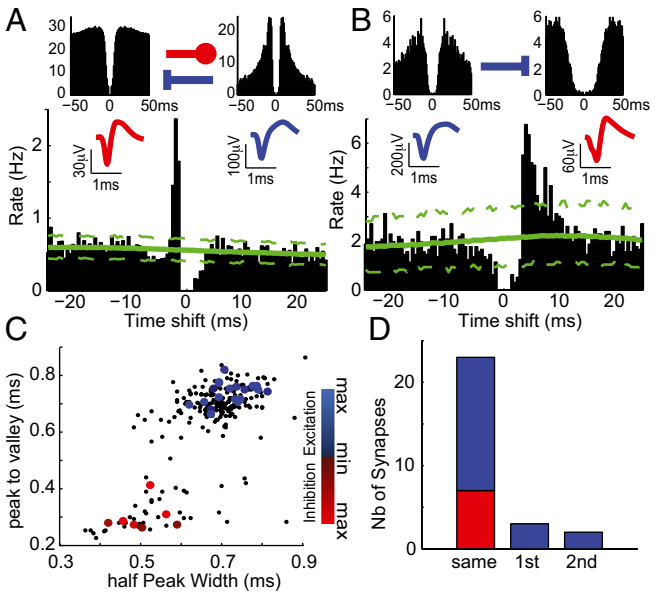

Fig. 3. Putative monosynaptic connections reflect neuronal type. (*A*) Cross-correlogram (*Lower*, referenced to firing by the putative Int) implies reciprocal monosynaptic interactions between an FS Int and an RS Pyr cell identified by their autocorrelograms (*y*-axis display rate in Hz) and spike waveforms (*Upper Left* and *Upper Right*, respectively). The large peak in the cross-correlogram indicates that the putative Pyr cell is systematically firing ~2 ms before the putative FS Int. Conversely, the decreased firing for 4 ms after the putative Int firing suggests that it inhibits the putative Pyr cell. Dashed green lines show the 99% confidence interval from jittered spike trains. (*B*) In this example a putative Pyr cell (reference of the cross-correlogram) tended to excite a putative Int at a latency of ~3 ms. In *A* and *B*, cells were recorded on the same electrodes; because of the nature of spike detection, the central values of the cross-correlograms are thus null. (*C*) The sign and strength of the putative monosynaptic connections were matched to the spike's average waveform. Small dots, all neurons; large dots, identified cell that appeared to monosynaptically affect another cell. Color code for sign (blue, excitation; red, inhibition) and strength (dark, weak; light, strong) of the connection. (*D*) Total number of synaptic connections between pairs of cells recorded by the same first- or second-neighbor electrodes.

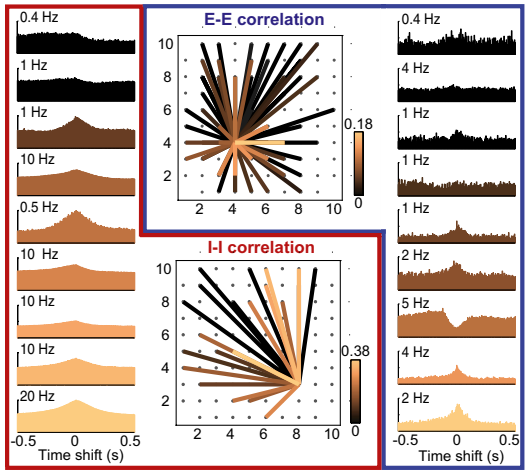

Fig. 4. Spatial distribution of cell–cell interactions in an example 2D recording session. (*Center Upper*) Correlation values of one putative Pyr cell with all others. Color codes for the absolute value of Pearson's correlation (calculated for 50-ms bins), with black indicating low correlation and copper indicating high. (*Right*) Randomly chosen cross-correlograms between the reference cell and nine others sorted by correlation values. The *y* axis displays instantaneous rates of target cells. (*Center Lower*) Correlations between one putative Int and all others. (*Left*) Sample Int–Int cross-correlograms.

The monosynaptic connectivity matrix was typically sparse. In the dataset, only 0.17% of the possible connections (28 of 16,932) showed a significant monosynaptic effect in the cross-correlograms. This result was not different for postsynaptic excitation and inhibition (respectively, 0.16% and 0.19% of the total numbers of possible postsynaptic contacts from Pyr or Int cells; $P > 0.05$, binomial test). Monosynaptic contacts were almost entirely local, 76% (16 of 21) of excitatory effects, and the totality of inhibitory ones was confined to pairs recorded on the same electrode (Fig. 3*D*); 5.65% of the possible contacts on pairs from same electrode showed a significant bias in the cross-correlograms. Based on this functional categorization, throughout the rest of the paper, we interchangeably use FS, inhibitory, and Int. Similarly, we do the same for RS, excitatory, and Pyr.

Spatiotemporal Dynamics of Cell Interaction. To investigate the interaction at the maximum possible spatial scale (i.e., ~4 mm), we correlated the binned spike trains at various timescales. This approach provides a spatiotemporal view of cell–cell interaction, mono- or polysynaptically. Fig. 4, *Center Upper* and *Right* shows the strength of the absolute correlation between one example Pyr cell and all other Pyr cells: The strength of the correlation between Pyr cells seems to decrease with distance. The absolute Pearson's correlation coefficients were directly related to peak or trough in the cell's cross-correlograms for different randomly chosen Pyr cells (Fig. 4, *Right*) in reference to the spike trains of the example cell from Fig. 4, *Center Upper*. Conversely, for Int (Fig. 4, *Center Lower* and *Left*), the correlation between cell pairs appeared to be independent of the distance separating the two cells. Also, unlike for Pyr cells, the degree of modulation of the cross-correlograms did not appear to be related to the size of Pearson's correlation, possibly because of the dependence of correlation coefficients on cell-intrinsic firing rates (22).

To further analyze the relationship between correlation and spatial arrangement of the cells, all of the cell pairs from the datasets were pooled together, and the absolute coefficients of correlation, computed with 50-ms time bins, were plotted as a function of interelectrode distance (Fig. 5*A*). To remove bias caused by firing-rate inhomogeneity in correlation values and to render Pyr–Pyr correlation coefficients comparable to those of Int pairs, correlations were then normalized by the geometric mean of each cell pair's average firing rates (22). Furthermore, to avoid experiment-dependent spurious covariation, which may, for example, arise from electrode drift, a local version of correlation was used (*SI Materials and Methods*). This analysis revealed that, first, the correlation between cell pairs recorded from the same electrode depended on their connectivity: As expected, putative monosynaptically connected pairs—whatever the nature of the synapse(s)—showed significantly higher absolute correlation than did nonconnected pairs (Fig. S2), revealing fine-scale structure in local microcircuits. Second, at the level of the whole recording matrix, the cell pairs were divided in two categories: putative inhibitory Int pairs (designated as the I–I group) and excitatory Pyr pairs (E–E group). Because of the improbability of an equal sampling ratio of the recorded Int and Pyr cells to the existent cells in the examined tissue, the E–I comparison does not hold the same validity as do E–E and I–I comparisons of correlation and therefore is not reported here. The linear regression between absolute correlations and distance between recording sites showed a negative slope for both groups but was significant only for the E–E group. Furthermore, when the same analysis was carried out for different time bin sizes (Fig. 5*B* and Fig. S3), the negative slope of the linear regression was significant ($P < 0.05$, Pearson's correlation test) across all timescales for the E–E group, but not for the I–I group. To ensure that the oversampling of Pyr cells compared with Int did not yield the difference in the significance levels, the number of Pyr

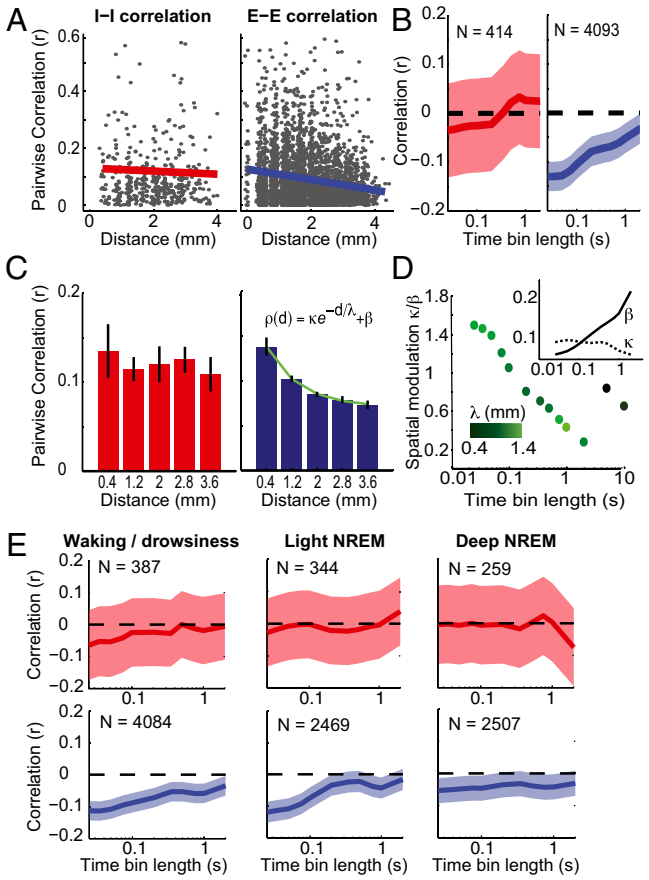

Fig. 5. Relation of firing correlation to distance between cells. (*A*) Normalized coefficients of correlations were plotted against the distance between the two cells in each pair of putative Int (I–I correlations, *Left*) and putative Pyr (E–E correlations, *Right*) cells computed on time bins of 50 ms. Only the E–E group shows a significant linear regression (red and blue lines). (*B*) Correlation values of linear regressions for different time bins. Shaded areas indicate the 95% confidence interval (Fisher method). Numbers of cell pairs are indicated for the two populations. (*C*) Same as in *A* but normalized correlation coefficients were averaged over 0.8-mm spatial intervals. For E–E connections, the decay is well fitted with an exponential. (*D*) Strength and extent of spatial modulation of E–E correlations relative to the time bin width. Strength of spatial modulation is estimated with the dimensionless quantity κ/β. Green intensity codes for spatial extent of the modulation (λ). (*Inset*) Values (*y* axis) of the fitting parameters β (solid line) and κ (dotted line) in function of time bin length (*x* axis). (*E*) Same as in *B* but in different wake/sleep states. Analyses were restricted to cells with mean firing rate > 0.3 Hz in each particular state, resulting in the different numbers of cell pairs as indicated.

pairs was down-sampled to match the number of Int pairs and bootstrapped. The correlation between neuronal pairwise correlation and distance remained significantly lower than 0 for time bins smaller than 200 ms (Fig. S4).

Next, the correlation values were averaged in equally spaced 0.8-mm intervals of interelectrode distance (Fig. 5*C*). The relationship between correlation and spatial distance was approximately flat in the I–I group, thus confirming the lack of a significant relationship. The E–E correlations decayed with distance and were well fit with a three-parameter exponential (Fig. 5*D*). The fitting parameters can be reduced to two meaningful values: the spatial extent of the exponential λ and the relative (dimensionless) amplitude modulation κ/β that quantifies the amplitude of the decay relatively to the baseline. κ/β decreased monotonically with time bin widths, whereas the spatial constant λ was more or less constant, with an average value of ∼1 mm. Notice that such decay did not sustain for time bins longer than 2 s (the two far right points in Fig. 5*D*). This decay resulted from a monotonic increase in the baseline correlation β and from a decrease of the exponential amplitude κ (Fig. 5*D*, *Inset*; values diverged for time bins longer than 2 s). Similar results were yielded for nonnormalized coefficients of correlation (Fig. S5).

State-Dependent Long-Range Correlation. Finally, we investigated the difference in spatial correlation between different states (Fig. 5*E*). Clear periods of light and deep non-rapid eye movement (NREM) sleep were detected in addition to wake/drowsiness epochs in two of the three patients (three recording sessions, representing 87% of the total discriminated cells in the analysis). The rapid eye movement (REM) episodes were brief, if detectable at all. For Int pairs, the linear regression between neuronal pairwise correlation and distance was never different from 0. For Pyr pairs, this correlation was highly significant for wake/drowsiness and light NREM over almost all tested time bin sizes. During deep NREM, the correlation was smaller for the different time bins but was still significant, or very close to significance, for most comparisons.

Discussion

The present paper reports a detailed quantitative analysis of the dynamics of excitation and inhibition in the human neocortex during overnight sleep. In particular, using massive cell recordings we have shown (*i*) robust morphological (extracellular waveform features) discrimination of putative cortical excitatory and inhibitory neurons; (*ii*) in vivo evidence of functional monosynaptic connections in the human neocortex; (*iii*) functional behavior of inhibitory and excitatory cells during human sleep; (*iv*) distinctive spatiotemporal patterns of Pyr–Pyr and Int–Int assembly interactions; and (*v*) detailed quantification of corticocortical correlations. Hence, this paper provides a unique insight to the dynamics of human neocortical microcircuits.

Separating Excitation from Inhibition. Different attempts were carried out recently to distinguish between putative Int and Pyr cells, for example, in the hippocampal formation (23). In nonprimates, the separation between the two populations on the basis of extracellular features is now generally accepted (13, 14). In this paper, human neocortical cell recordings were clustered on their extracellular waveforms. The two parameters describing waveform morphology formed well-defined clusters that were captured by standard algorithms (Fig. 2 and Fig. S1*A*). First, despite the a priori higher probability to detect the high-amplitude spikes from large Pyr cells, the overall proportion of cells in each group (80% Pyr and 20% Int) was consistent with the known ratio between Pyr and Int cells in the neocortex (24). In other words, a random sampling with extracellular electrodes gives rise to the expected distribution of cell types, thus indicating that they are both detectable with sufficient reliability. Second, this segregation was consistent over several other cell-intrinsic parameters, such as firing rates (higher for FS Int) or the high tendency of the Pyr cells to burst (Fig. 2).

As supplementary evidence of separation between Int and Pyr cells, we analyzed the potential monosynaptic interactions between cell pairs and categorized them as excitatory or inhibitory. The distribution of cells' postsynaptic effects perfectly matched the clustering of excitatory and inhibitory cells based on their extracellular features (Fig. 3).

Overall firing rates were surprisingly low, <0.5 Hz for the RS cells and ∼2 Hz for the FS cells. However, using long-lasting recordings allowed us to reliably isolate the cells' spikes during cluster-cutting procedures, even if those were sometimes very rare, whereas those low firing-rate cells could have been disregarded in other situations. This low firing rate may relate to the recordings being in superficial layers because animal studies have demonstrated that many of these neurons have lower firing rates

than in the deep layers (25). It is also consistent with other recordings in human neocortex (11) and may reflect fundamental metabolic constraints in large brains (26).

Theoretical studies have emphasized that, in a sparsely connected network, the seemingly irregular firing of cells could be the consequence of the balance between excitation and inhibition (27–29). Similarly, intracellular recordings have revealed a balance between excitatory and inhibitory conductance both in vitro (30) and in vivo (31), they and even shown a possible excess of inhibition in vivo (32). However, inhibitory cells are four to five times less common than excitatory cells, as are the number of synapses they form onto postsynaptic targets (24). Although direct demonstration of balanced excitation and inhibition requires intracellular recordings, our extracellular analysis provides indirect evidence in favor of such a balance. First, the average firing rate of Int was five times higher than that of Pyr cells (Fig. 2), which is the same ratio as the total number of cells from each type. Second, it has been shown theoretically that balanced networks exhibit a heavy-tailed, wide range of firing rates (27), which was found to be the case for the human neurons recorded here, where, for both Pyr and Int, the firing rates were log-normally distributed (Fig. 2).

Spatiotemporal Extent of Neuronal Interrelationships. The interaction between neocortical neurons takes place at different spatiotemporal scales, and this paper sheds light on such interactions in human neocortex. We found that the short-latency monosynaptic effects from spike-train cross-correlograms were confined to the same or very proximal electrodes (Fig. 3*D*), in agreement with the rapid decrement with distance of synaptic contact probability (24, 33). The extent of monosynaptic contacts in local circuits is still a subject of debate (1, 2, 24, 33), and it is important to bear in mind that spike-train correlation analysis (33) is likely to underestimate the number of actual contacts because it is based only on suprathreshold activity from pre- and postsynaptic neurons.

The connected cells showed higher long-timescale correlations than the cells recorded from the same electrodes without any detectable synaptic contact (Fig. S2). This finding suggests that connected units tend to participate in the same cell assemblies (34) and echoes the recent findings that suggest that those units are more likely to receive common inputs within the cortical column (1).

We also found that the binned spike-train correlations showed spatial dependence only for excitatory cell pairs, whereas inhibitory cell pairs were as much correlated with both proximal and distal electrodes over the 4-mm extent of the array. For the Pyr cell pairs, the modulation of the spatial extent decreased with the timescale at which correlations were computed; however, the spatial constant of this decay (~1 mm) was approximately the same, independent of the timescale (Fig. 5 and Fig. S3).

These results have strong implications for our understanding of cortical network dynamics. First, the neuronal activity of Pyr cells remains coherent on a scale corresponding to the spatial extent of the axonal arborization in superficial layers. This is also the same spatial extent of a typical "hyper-columnar" organization of human neocortex (24), robustly described in primary sensory cortices and less in higher-order areas such as the temporal neocortex. Second, the correlations tended to equalize, as measured by the spatial-modulation factor, for longer timescales. This is a known result from neocortical LFPs that shows high spatial correlation over a large proportion of the network during slow wave activity (5, 35) (characterized by long-timescale dynamics) compared with low spatial correlation during states dominated by short timescales exhibiting desynchronized, low-amplitude, and fast oscillations (36). Accordingly, when the relationship between Pyr pairwise correlations and distance was investigated separately for the different wake/sleep states, the main difference was the decrease of this relationship during deep NREM sleep, although still significant (Fig. 5*E*), presumably because of the widespread entrainment of neuronal activity by slow/δ oscillations.

Conversely, the large spatial extent of interneuronal correlations could be caused by common subcortical inputs over large neocortical areas impinging directly onto GABAergic cells, as can be the case for thalamocortical (37, 38) projections. In addition, the highly complex distribution of interneuronal connectivity, with some cells contacting very distant areas, could produce large-scale synchronization of the inhibitory network (39).

It is important to keep in mind that these recordings were made in epileptic patients, and, although the present analyses were done in periods of activity devoid of seizures or activity on either the microelectrode array or any subdural electrode, we cannot eliminate the possibility that some of our results may reflect a pathological rearrangement of neuronal numbers and/or interconnections.

The current results suggest that neocortical principal cells may be organized into coherent firing units, or cell assemblies, mainly on the basis of local excitatory interactions (~1 mm). In parallel, the inhibitory network maintains coherent activity over much larger distances (>4 mm). The role of such large-scale synchronized inhibition should be investigated by future studies. These results constitute an initial step toward understanding the dynamic and functional microarchitecture of human neocortical circuits, characterized by spatiotemporal interactions spanning several orders of magnitude.

Overall, this paper not only extends the prior work reported in animals to the human cortex but also tackles it with an exhaustive quantification that can be verified in future studies (in animals as well as in humans) and will prove useful in the interpretation of the many studies, published and underway, that explore the details of human single neurons during cognition, sleep, seizures, and a wide range of other situations.

Materials and Methods

Recordings were made from three patients (ages 21, 24, and 52 y; two women and one man). All patients had focal epilepsy arising from differing causes: a cortical dysplasia, a glioneural tumor, or postencephalitic cortical gliosis and hippocampal sclerosis as confirmed by postoperative histology. The NeuroPort electrode array, 1 mm in length, was placed in layers II/III of the middle temporal gyrus in all three patients. This array is silicon-based, made up of 96 microelectrodes with 400-μm spacing, covering an area of 4 × 4 mm (40). A total of four nights of natural sleep were examined (one night for two of the patients, two nights for the other patient). Data were sampled at 30 kHz (Blackrock Microsystems). The implantation site was included in the therapeutic resection in all patients. Recordings were made in 40-min segments, which were concatenated over a given night for spike sorting. Single units were discriminated by using standard clustering methods (*SI Materials and Methods*). On average, 57% (±12%) of the electrodes showed visible neuronal activity, including electrodes that were not possible to cluster: Individual cells were isolated from 75% (±14%) of these electrodes. On average, 1.39 (±0.26) neurons were discriminated from each electrode where at least one neuron was isolated.

See *SI Materials and Methods* for further details.

ACKNOWLEDGMENTS. This research was supported by the Centre National de la Recherche Scientifique, Agence Nationale de la Recherche HR-Cortex project, European Community Future and Emerging Technologies program Fast Analog Computing with Emergent Transient States (FACETS) Grant FP6-015879 and BrainScaleS (Brain-Inspired Multiscale Computation in Neuromorphic Hybrid Systems) Grant FP7-269921, and National Institutes of Health Grants 5R01NS062092 and R01 EB009282. N.D. is supported by a fellowship from Ecole des Neurosciences de Paris, and A.P. is supported by a postdoctoral fellowship from the European Molecular Biology Organization.

1. Yoshimura Y, Dantzker JLM, Callaway EM (2005) Excitatory cortical neurons form fine-scale functional networks. *Nature* 433:868–873.
2. Song S, Sjöström PJ, Reigl M, Nelson S, Chklovskii DB (2005) Highly nonrandom features of synaptic connectivity in local cortical circuits. *PLoS Biol* 3:e68.
3. Ohiorhenuan IE, et al. (2010) Sparse coding and high-order correlations in fine-scale cortical networks. *Nature* 466:617–621.
4. Buzsáki G, Draguhn A (2004) Neuronal oscillations in cortical networks. *Science* 304: 1926–1929.

5. Steriade M (2003) *Neuronal Substrates of Sleep and Epilepsy* (Cambridge Univ Press, Cambridge, UK).
6. Wiebe S, Blume WT, Girvin JP, Eliasziw M; Effectiveness and Efficiency of Surgery for Temporal Lobe Epilepsy Study Group (2001) A randomized, controlled trial of surgery for temporal-lobe epilepsy. *N Engl J Med* 345:311–318.
7. Fried I, et al. (1999) Cerebral microdialysis combined with single-neuron and electroencephalographic recording in neurosurgical patients. Technical note. *J Neurosurg* 91:697–705.
8. Patterson WR, et al. (2004) A microelectrode/microelectronic hybrid device for brain implantable neuroprosthesis applications. *IEEE Trans Biomed Eng* 51:1845–1853.
9. Waziri A, et al. (2009) Initial surgical experience with a dense cortical microarray in epileptic patients undergoing craniotomy for subdural electrode implantation. *Neurosurgery* 64:540–545, discussion 545.
10. Cash SS, et al. (2009) The human K-complex represents an isolated cortical downstate. *Science* 324:1084–1087.
11. Csercsa R, et al. (2010) Laminar analysis of slow wave activity in humans. *Brain* 133: 2814–2829.
12. Le Van Quyen M, et al. (2010) Large-scale microelectrode recordings of high-frequency gamma oscillations in human cortex during sleep. *J Neurosci* 30:7770–7782.
13. Barthó P, et al. (2004) Characterization of neocortical principal cells and interneurons by network interactions and extracellular features. *J Neurophysiol* 92:600–608.
14. McCormick DA, Connors BW, Lighthall JW, Prince DA (1985) Comparative electrophysiology of pyramidal and sparsely spiny stellate neurons of the neocortex. *J Neurophysiol* 54:782–806.
15. Le Van Quyen M, et al. (2008) Cell type-specific firing during ripple oscillations in the hippocampal formation of humans. *J Neurosci* 28:6104–6110.
16. Truccolo W, et al. (2011) Single-neuron dynamics in human focal epilepsy. *Nat Neurosci* 14:635–641.
17. Keller CJ, et al. (2010) Heterogeneous neuronal firing patterns during interictal epileptiform discharges in the human cortex. *Brain* 133:1668–1681.
18. Smith MA, Kohn A (2008) Spatial and temporal scales of neuronal correlation in primary visual cortex. *J Neurosci* 28:12591–12603.
19. Hirase H, Leinekugel X, Csicsvari J, Czurkó A, Buzsáki G (2001) Behavior-dependent states of the hippocampal network affect functional clustering of neurons. *J Neurosci* 21:RC145.
20. Schevon CA, et al. (2008) Microphysiology of epileptiform activity in human neocortex. *J Clin Neurophysiol* 25:321–330.
21. Silverman BW (1981) Using kernel density estimates to investigate multimodality. *J R Stat Soc B* 43:97–99.
22. de la Rocha J, Doiron B, Shea-Brown E, Josić K, Reyes A (2007) Correlation between neural spike trains increases with firing rate. *Nature* 448:802–806.
23. Viskontas IV, Ekstrom AD, Wilson CL, Fried I (2007) Characterizing interneuron and pyramidal cells in the human medial temporal lobe in vivo using extracellular recordings. *Hippocampus* 17:49–57.
24. Braitenberg V, Schüz A (1998) *Cortex: Statistics and Geometry of Neuronal Connectivity* (Springer, Berlin).
25. Sakata S, Harris KD (2009) Laminar structure of spontaneous and sensory-evoked population activity in auditory cortex. *Neuron* 64:404–418.
26. Lennie P (2003) The cost of cortical computation. *Curr Biol* 13:493–497.
27. van Vreeswijk C, Sompolinsky H (1996) Chaos in neuronal networks with balanced excitatory and inhibitory activity. *Science* 274:1724–1726.
28. Amit DJ, Brunel N (1997) Model of global spontaneous activity and local structured activity during delay periods in the cerebral cortex. *Cereb Cortex* 7:237–252.
29. Renart A, et al. (2010) The asynchronous state in cortical circuits. *Science* 327:587–590.
30. Shu Y, Hasenstaub A, McCormick DA (2003) Turning on and off recurrent balanced cortical activity. *Nature* 423:288–293.
31. Haider B, Duque A, Hasenstaub AR, McCormick DA (2006) Neocortical network activity in vivo is generated through a dynamic balance of excitation and inhibition. *J Neurosci* 26:4535–4545.
32. Rudolph M, Pospischil M, Timofeev I, Destexhe A (2007) Inhibition determines membrane potential dynamics and controls action potential generation in awake and sleeping cat cortex. *J Neurosci* 27:5280–5290.
33. Fujisawa S, Amarasingham A, Harrison MT, Buzsáki G (2008) Behavior-dependent short-term assembly dynamics in the medial prefrontal cortex. *Nat Neurosci* 11: 823–833.
34. Harris KD (2005) Neural signatures of cell assembly organization. *Nat Rev Neurosci* 6: 399–407.
35. Achermann P, Borbély AA (1998) Coherence analysis of the human sleep electroencephalogram. *Neuroscience* 85:1195–1208.
36. Destexhe A, Contreras D, Steriade M (1999) Spatiotemporal analysis of local field potentials and unit discharges in cat cerebral cortex during natural wake and sleep states. *J Neurosci* 19:4595–4608.
37. Jones EG (2007) *The Thalamus* (Cambridge Univ Press, Cambridge, UK).
38. Contreras D, Destexhe A, Steriade M (1997) Intracellular and computational characterization of the intracortical inhibitory control of synchronized thalamic inputs in vivo. *J Neurophysiol* 78:335–350.
39. Buzsáki G, Geisler C, Henze DA, Wang XJ (2004) Interneuron Diversity series: Circuit complexity and axon wiring economy of cortical interneurons. *Trends Neurosci* 27: 186–193.
40. Campbell PK, Jones KE, Huber RJ, Horch KW, Normann RA (1991) A silicon-based, three-dimensional neural interface: Manufacturing processes for an intracortical electrode array. *IEEE Trans Biomed Eng* 38:758–768.